



Application of neural network modelling for classifying hydrocarbon bearing zone, water bearing zone and shale with estimation of petrophysical parameters in Cauvery basin, India

ATUL KUMAR PANDEY¹, RIMA CHATTERJEE^{1,*} and BISWAJIT CHOUDHURY^{1,2}

¹Department of Applied Geophysics, Indian Institute of Technology (Indian School of Mines), Dhanbad 826 004, India.

²Present address: Geological Survey of India, Jaipur, India.

*Corresponding author. e-mail: rima_c_99@yahoo.com

MS received 12 March 2019; revised 6 August 2019; accepted 13 August 2019

This work has been developed to classify sand and shale from seven wells in the Cauvery basin using a multilayered feedforward neural network (MLFN) model. Seven wells distributed over 5100 km² of this basin have been utilized for analysis of conventional well logs and reservoir characterization. Hydrocarbon bearing sediments of Andimadam, Bhuvanagiri, Nannilam and Niravi formations of the Cauvery basin are evaluated in terms of shaliness, cementation factor, porosity, water saturation, and permeability. Pickett plot has been applied to investigate the cementation factor, formation water resistivity, permeability. The cementation factor (m) varies from 1.31 to 1.86 in these formations, whereas permeability varies from 0.01 to 400 md. Very good quality reservoir exists in the Bhuvanagiri formation with high permeability 300–400 md, whereas a good quality reservoir is occurring in Niravi, Nannilam and Andimadam formations with hydrocarbon saturation 60–70%.

Keywords. Porosity; permeability; cementation factor; neural network model; Cauvery basin.

1. Introduction

Identification of hydrocarbon bearing zone and estimation of the petrophysical parameters associated with it, namely, water saturation, the volume of shale, cementation factor, porosity, and permeability are essential for the determination of flow unit. The physical properties of sediments like natural radioactivity, resistivity, density, compressional/shear sonic travel time, neutron porosity commonly measured through geophysical logging, are used for identification of fluid and lithology of hydrocarbon bearing sand reservoir (Singha and Chatterjee 2017; Das and Chatterjee

2018). Several authors have classified mud-rocks, siliciclastic, coal and coal proxi parameters from conventional well logs using the neural network (Baldwin *et al.* 1990; Bhatt and Helle 2002; Maiti *et al.* 2007; Schmitt *et al.* 2013; Ghosh *et al.* 2016). The available geophysical log responses are observed in wells at the Cauvery basin. The purpose of this study is to classify the hydrocarbon bearing zone, water bearing zone and shale using a multilayered feedforward neural network (MLFN) model. We have further estimated the cementation factor, porosity, permeability and water saturation of hydrocarbon bearing zones of wells drilled in this basin.

Typically conventional logs (such as density, neutron and sonic logs) are used to estimate porosity, but permeability estimation requires the study of core samples. However, in the absence of core data, well log data may be used for the computation of permeability. Pickett plot (resistivity *vs.* porosity) is generally used to characterize the behaviour of reservoir flow units (Martin *et al.* 1997; Aguilera and Aguilera 2002; El-Khadrag *et al.* 2014). Sanyal and Ellithorpe (1978) and Greengold (1986) had demonstrated computation of the cementation factor (m) from the Pickett plot. This paper describes the MLFN model for the identification of hydrocarbon bearing zones and the uses of Pickett plot (Aguilera 2001) for computation of reservoir parameters such as the cementation factor, formation water resistivity, water saturation, permeability from eight wells of Cauvery basin.

2. Study area

The Cauvery basin extending along the east coast of India, has been formed as a pericratonic rift basin due to fragmentation of Gondwanaland during drifting of India–Sri Lanka landmass system away from Antarctica/Australia plate in Late Jurassic/Early Cretaceous (Prabhakar and Zutshi 1993; Saha *et al.* 2008; Phaye *et al.* 2011). The basin exhibits a series of parallel horsts and grabens structures trending NE–SW direction formed due to rifting (figure 1). Exploratory drilling in this basin revealed more than 6 km thick deep marine clastic sediments of Mesozoic and Cenozoic age with multiple reservoirs holding commercial hydrocarbon. The generalized lithostratigraphy of the Cauvery basin interpreted from the available seismic section with age varying from Pre-Cambrian to Miocene is shown in figure 2 (Venkatarengan *et al.* 1993). Eight wells: CBV, CPT, CKL, CMT, CNL, CPV, CKP and CKK are distributed covering 5100 km² area of the Cauvery basin (figure 1). The well log correlation using gamma ray and resistivity logs (Rider 2002; Eichkitz *et al.* 2009) through seven wells: CBV, CPT, CKL, CMT, CNL, CKP and CKK across section AA' is shown in figure 3 (Choudhury *et al.* 2015). Top of formations are marked on the basis of gamma ray and deep resistivity log characteristics.

3. Well log analysis

Geological formations such as: Andimadam, Sattapadi Shale, Bhuvanagiri, Kudavasal Shale, Nannilam, Portonovo Shale, Kamalapuram,

Karaikal Shale, Niravi Sandstone of age ranging from Lower Cretaceous to Middle Miocene as described in figure 2 are evaluated using conventional well log analysis. Multimineral lithologies consisting of sandstone, limestone, dolomite and shale exist in the sediments penetrated through eight wells under the study area. Gamma ray logs measure the radioactivity of formations in the well which indicates the presence of clay mineral, oil source rock, organic matter and shale in reservoir rock (Schlumberger 1972). Sandstones (hydrocarbon or water bearing), have a low concentration of radioactive elements thus registering a low gamma ray count. The gamma ray (GR) values in these hydrocarbon bearing zones of wells CMT, CKK, CBV, CNL, CPV and CPT range from 20.39 to 70 API.

Resistivity is the property of a material or substance to resist the flow of electric current through material (Schlumberger 1972). Three types of resistivity logs are available which are, flushed zone resistivity (micro spherically focused, MSFL), shallow resistivity (laterolog shallow, LLS) and deep resistivity (laterolog deep, LLD). LLD and LLS logs show a higher value than MSFL logs in hydrocarbon bearing zones. The deep resistivity log response in hydrocarbon bearing zones as observed from six wells ranges from 4.0 to 874.0 Ω m. As gas concentration increases, the separation between MSFL and LLD/LLS also increases. In the case of water saturation, all resistivity curves coincide with each other.

Density log is strongly affected by the presence of gas and records the lowest density values in gas saturated sand. The neutron porosity tool accounts for the amount of hydrogen present in the formation. In clean sandstone formations, where porosity is filled with water or oil, the neutron log measures liquid-filled porosity. Neutron log response becomes high in shale because of the presence of clay bound water, whereas it shows a very low value in gas saturated sand.

The gas bearing zone is indicated when the neutron porosity is less than the density porosity in a porous and permeable zone. This separation between neutron and density, termed as a crossover, is an indicator of gas bearing zones in clean sand (Bateman 1985). The crossover effect becomes smaller suggesting the presence of oil saturated sand. Water saturated sand is represented by overlaying of neutron and density logs (Singha and Chatterjee 2017; Das and Chatterjee

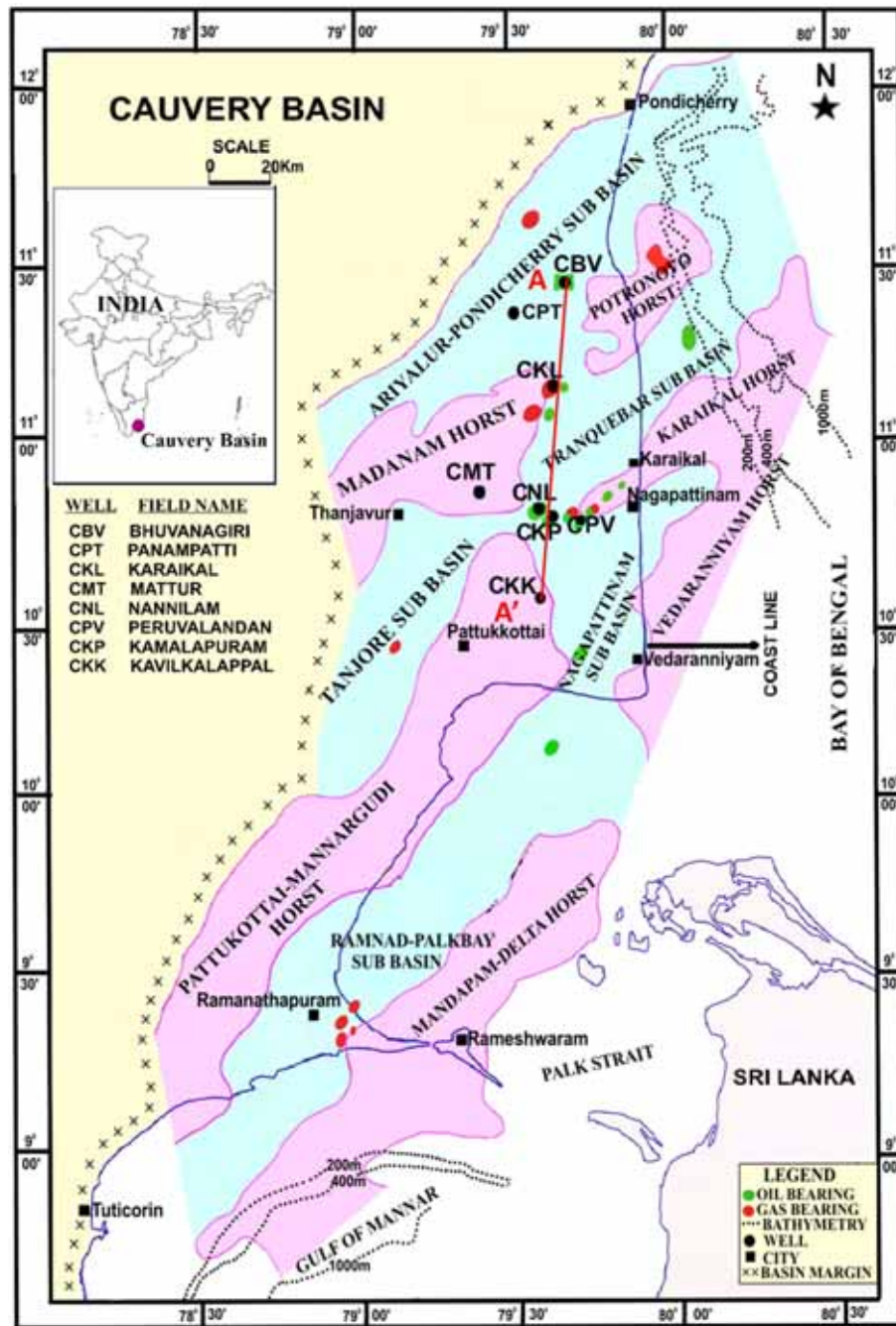


Figure 1. The tectonic framework of the Cauvery basin. Eight wells are distributed in oil/gas fields of this basin (after Prabhakar and Zutshi 1993; Choudhury *et al.* 2015).

2018). The typical well log responses for water bearing zone, hydrocarbon saturated zone and shale are illustrated through figure 4(a and b) for wells CMT and CNL, respectively. The hydrocarbon bearing zones are delineated from neutron-density crossover and the separation between deep (RD), shallow (RS) and flushed zone (Rxo) resistivity logs. The multilayered neural network approach is to be used for identification of hydrocarbon bearing zone, water bearing zone and shale from seven wells under study area.

4. Multilayered Feed Forward Neural Network (MLFN) approach for identification of reservoir, water saturated zone and shale

Cross plotting techniques are available for identification of fluids and lithology using conventional logs for selected depth intervals (Singha and Chatterjee 2017; Das and Chatterjee 2018; Gogoi and Chatterjee 2019). Here, our aim is to identify hydrocarbon bearing zones from seven wells for

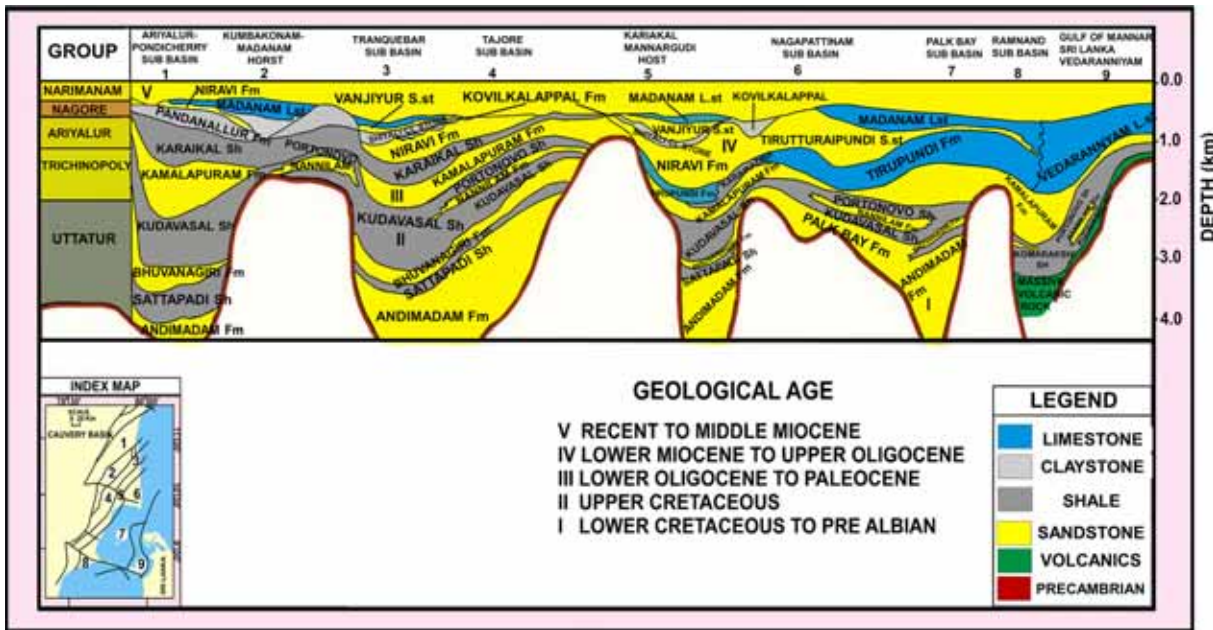


Figure 2. Generalized lithostratigraphy of Cauvery basin (after Venkatarengan *et al.* 1993).

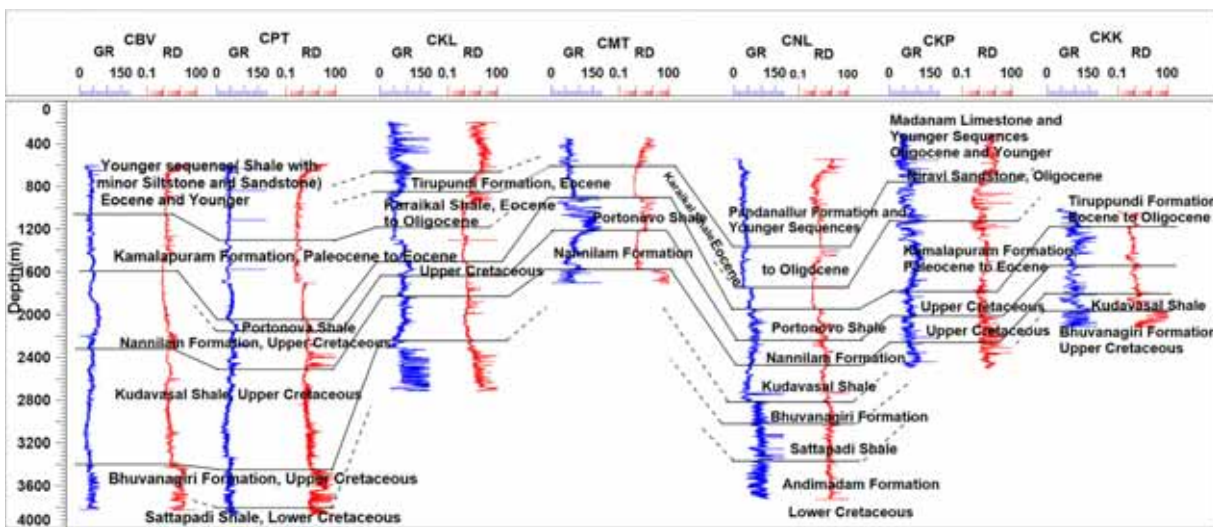


Figure 3. Illustrates well log correlation through AA' for seven wells. Gamma ray and resistivity logs are shown (Choudhury *et al.* 2015).

depth intervals varying from 300 to 3800 m. A quick look or cross plotting technique will be tedious and time consuming for identifying hydrocarbon bearing zones using conventional well log responses.

Estimation of lithology from well logs in heterogeneous formation is difficult to solve by the quick look interpretation method (Masoudi *et al.* 2011). Artificial neural network (ANN) tool has been successfully utilized for the determination of lithology using the transformation between well logs (Lim 2005; Singha *et al.* 2014; Chatterjee *et al.* 2016; Ghosh *et al.* 2016).

MLFN is a special arrangement of ANN that is the most precise method for solving the non-linear classification of lithology and bed boundaries identification problems (Maiti *et al.* 2007). In general, the architecture of an MLFN consists of one input layer, one output layer and at least one or two intermediate hidden layers between the input and output layer (Hampson *et al.* 2001). Here an MLFN model is created using geophysical log data, such as: GR, RD (Rt), flushed zone resistivity (R_{xo}), bulk density (Rho_b) and neutron porosity (Phin) as input parameters. Water saturated zone, hydrocarbon bearing zone and shale are considered as output

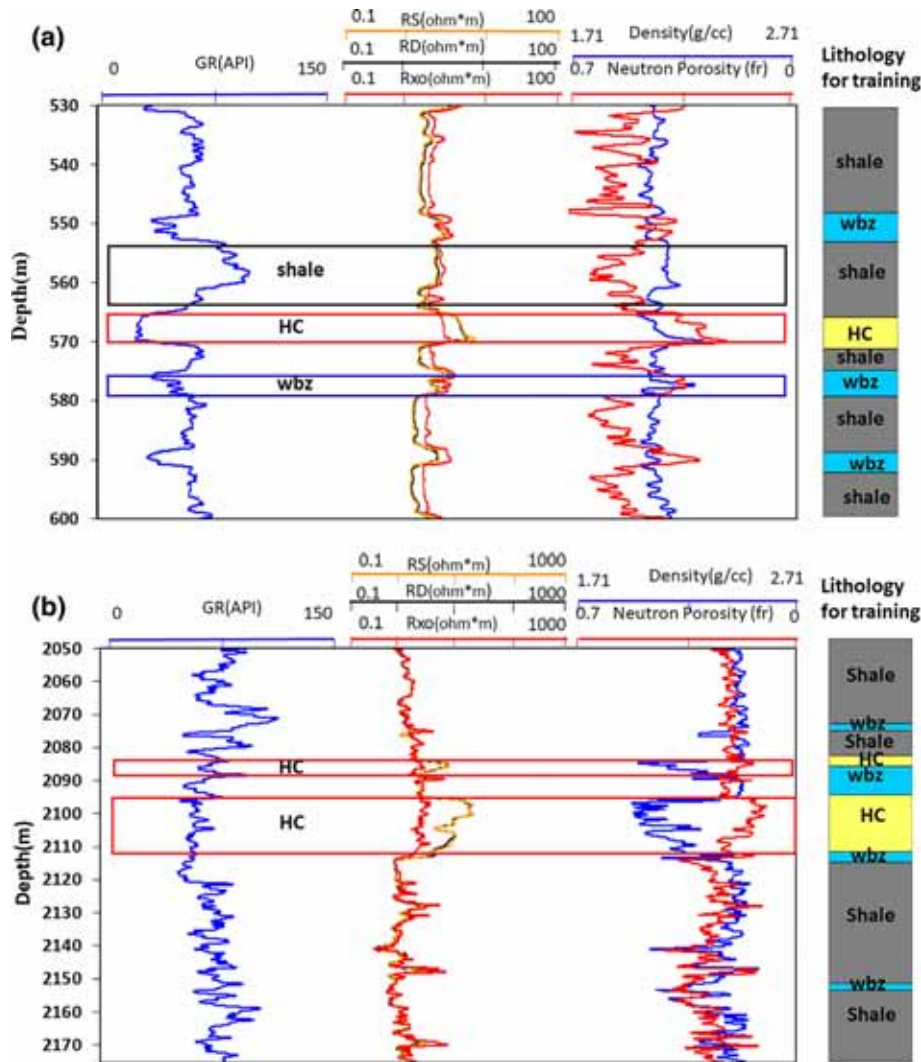


Figure 4. Typical conventional log responses in wells. (a) CMT and (b) CNL. Hydrocarbon bearing zone (HC) marked by rectangular shape by red, water bearing zone (wbz) by blue and shale by black colours, respectively. Observed lithology are provided against depths which are used to train the MLFN model.

parameters with double hidden layers (Masters 1994). In a fully connected MLFN, neurons of each layer are connected to the neurons of the next layer through some weight (Chatterjee *et al.* 2016; Ghosh *et al.* 2016). As shown in figure 5, the input layer constitutes of the input data for the nodes in hidden layers and output data of this hidden layer constitutes the input data for the output layer. Nodes are not connected within the same layer. For the training of the MLFN model, three lithocodes (10, 20 and 30) are assigned to hydrocarbon bearing zone, water bearing zone and shale, respectively, as output layers (Maiti *et al.* 2007; Ghosh *et al.* 2016). The selected depth intervals for two wells, CMT and CNL are used to train the model. The training dataset of 98 depth points have been chosen from depth intervals: 400–1700 m from well CMT, 2000–3700 m from well CNL, respectively. The selected depth intervals for

two wells, CMT and CNL are used to train the model. Hydrocarbon bearing zone, water bearing zone and shale are identified from log responses in these depth intervals (figure 4a and b). Hydrocarbon bearing zone is identified from 566.5 to 570.5 m in well CMT as well as from 2085 to 2112 m in well CNL. Water bearing zone is identified from 960 to 985 m in well CMT as well as from 2169 to 2175 m in well CNL. Shale is identified from 554 to 564 m in well CMT as well as from 3380 to 3389 m in well CNL. Table 1 shows the range of log responses for three lithocodes to train the MLFN model.

The network is trained with known lithocodes to develop an optimal set of weights between nodes (Chatterjee *et al.* 2016; Ghosh *et al.* 2016). The back-propagation algorithm (Dayoff 1990; Paul *et al.* 2018) uses a training pattern in which the first step is the forward propagation step followed

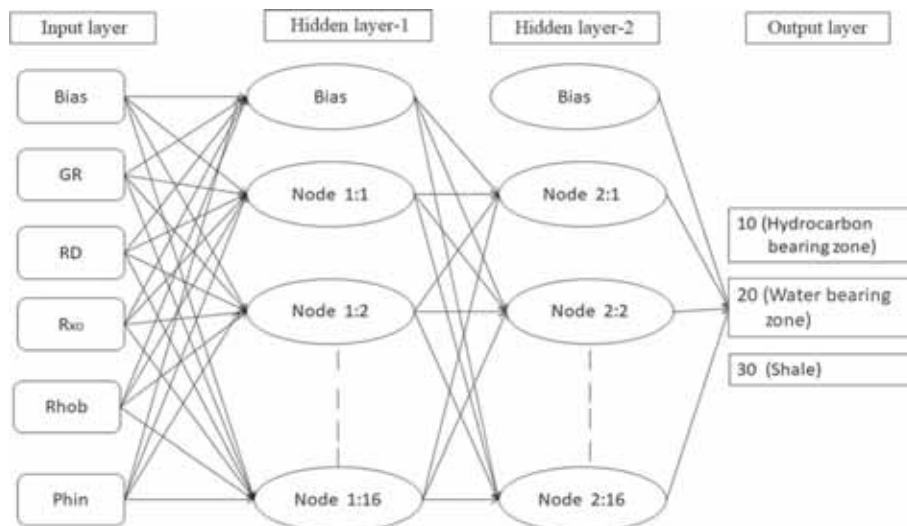


Figure 5. Schematic diagram for MLFN architecture for identification of hydrocarbon bearing zone.

Table 1. Range of log responses for three lithocodes to train the MLFN model.

Lithology unit	Gamma ray (API)	R_t (Ωm)	R_{xo} (Ωm)	Neutron porosity (Phin) (fr)	Density (Rhob) (gm/cc)	Lithocode
Hydrocarbon bearing zone	50.0–63.0	13.0–30.0	3.0–10.0	0.08–0.17	2.00–2.39	10
Water bearing zone	25.0–58.4	5.0–11.6	5.0–18.0	0.13–0.21	2.24–2.54	20
Shale	63.0–86.0	0.78–4.84	1.22–4.18	0.41–0.57	2.02–2.16	30

by the back-propagation step. The parameter at the output layer has been computed using the back-propagation technique as given below:

$$Y = f \left[\alpha_0 + \sum_{j=1}^{n_2} \alpha_j f_j \left(\beta_{oj} + \sum_{i=1}^{n_1} \beta_{ij} x_i \right) \right], \quad (1)$$

where Y is the output parameter, x is the input parameter, α and β are the connecting weights, n_1 is the dimension of the input vector, and n_2 is the number of hidden neurons. α_0 and β_{oj} are called the bias weights. The thresholding function (f) applied at the hidden node is typically a sigmoid function.

The general form of sigmoid function is

$$\text{sigmoid}(a) = 1/(1 + e^{-a}). \quad (2)$$

It squeezes its input (i.e., a) to a value between 0 and 1.

The problem of estimating the weights has been considered a nonlinear optimization problem, where the objective is to minimize the sum-squared error (SSE) between the observed lithocode and the MLFN predicted lithocode.

$$\text{SSE} = \sum_{i=1}^n (x_i - \bar{x})^2, \quad (3)$$

where, n is the number of observations, x_i is the value of the i th observation and \bar{x} is the mean of observations.

To initialize the hidden layer weights, SSE for a trial model is computed by repeating steps for 1000 epochs with 16 hidden nodes at the two hidden layers. The lowest value of SSE is chosen for the selection of weights to optimize the MLFN model (Paul *et al.* 2018). The network is trained with 70% of the total available data, then validated with the remaining 20% and then tested on 10% data using IBM SPSS version 21 software. The training dataset accounts for 70% of the entire dataset and is used to calculate errors and adjust connection weights and bias of network. The overtraining or over-fitting effect is avoided by using the validation dataset. Figure 6(a and b) displays the SSE *vs.* epoch for training and validation dataset. It is observed that the training error reaches a minimum at 600 epoch and then increases, whereas validation is minimum at 600 epoch and then starts undulating. Since it becomes minimum at 600 epoch, so the training is optimized with 600 epoch with 16 hidden nodes. Therefore, two hidden layers each consisting of 16 individual nodes with 600 epoch are best suited to present identification

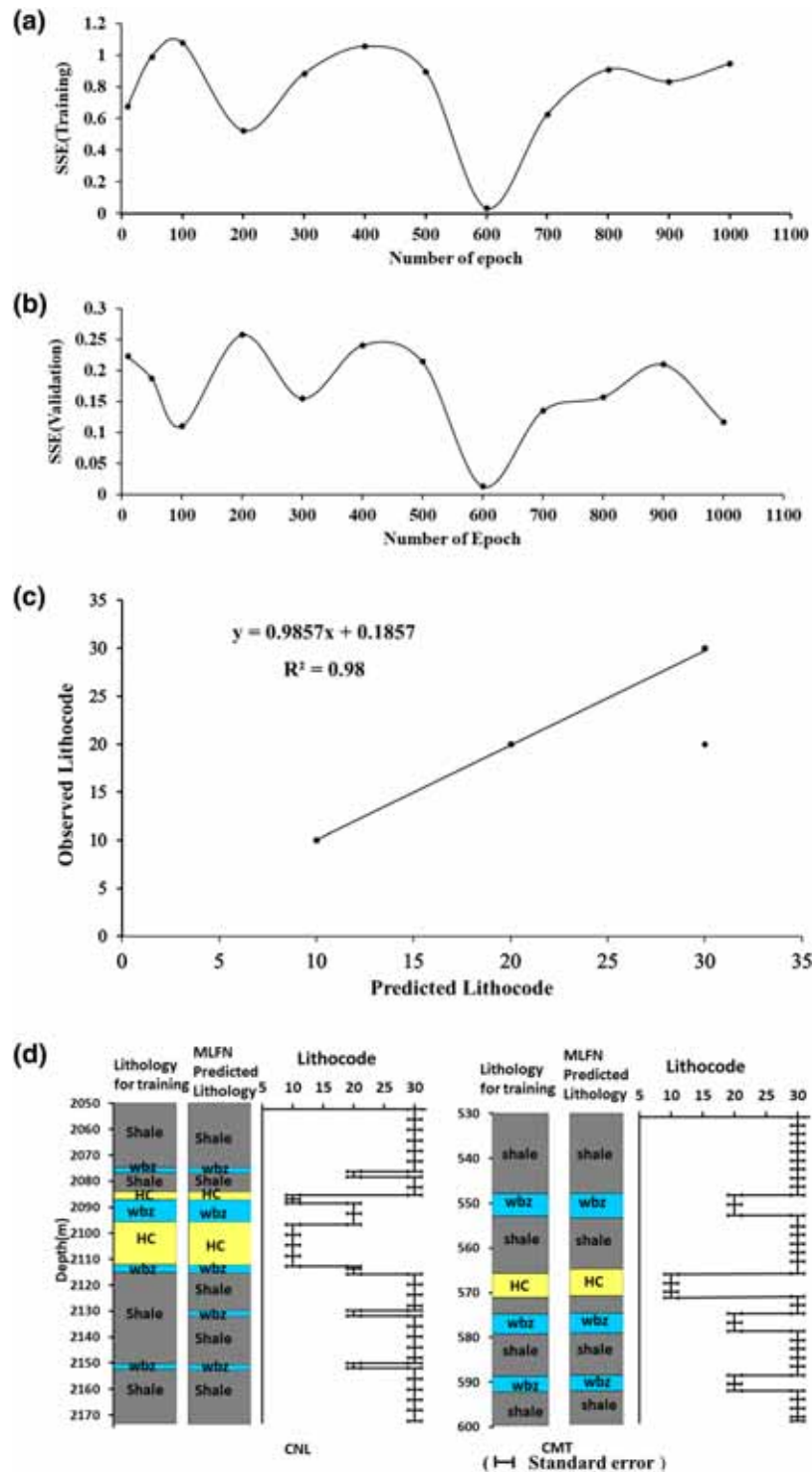


Figure 6. The sum square error (SSE) vs. epoch for (a) training dataset, (b) validation dataset, (c) relation between MLFN model predicted lithocode and observed lithocode for training dataset, (d) observed lithology and MLFN predicted lithology for training wells and their standard error bar with MLFN predicted lithology (standard error for CNL is 1.11 and for CMT is 0.94), and (e) observed lithology and MLFN predicted lithology for testing wells and their standard error bar with MLFN predicted lithology (standard error for CPV is 0.86 and for CKK is 0.88). HC: hydrocarbon bearing zone and wbz: water bearing zone.

problems as dictated by well log data. Figure 6(c) presents the relation between observed lithocode and predicted lithocode with the goodness-of-fit ($R^2 = 0.98$) for training the MLFN

model. Training dataset and MLFN predicted lithology for selected depth intervals of two wells: CNL (2050–2170 m) and CMT (530–600 m) are shown in figure 6(d). Testing dataset and MLFN

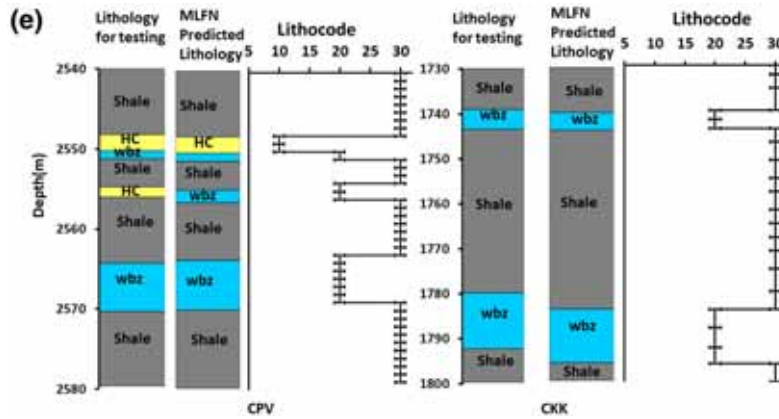


Figure 6. (Continued.)

predicted lithology for selected depth intervals of two wells: CPV (2540–2580 m) and CKK (1730–1800 m) are shown in figure 6(e).

Accuracy of prediction is justified with figure 6(c–e). A very good match is observed between the observed lithology and MLFN predicted lithology with excellent R^2 of 0.98 of the trained the MLFN model. Figure 6(d and e) indicate the MLFN predicted lithology corresponding to the log responses for training and testing wells with the observed lithology respectively.

The trained MLFN model is applied to the five wells for identification of hydrocarbon bearing zones for total depth interval varying from 300 to 3800 m. The model predicted results are listed in table 2. Figure 7(a) shows the MLFN predicted output for well CKK; figure 7(b–d) are the output for well CPV; figure 7(e) is for well CBV, for specific depth intervals (figure 7). Hydrocarbon bearing zones are identified in four wells namely; CKK, CPV, CBV and CPT. Hydrocarbon bearing zones are not detected in well CKP.

5. Estimation of petrophysical parameters

5.1 Pickett plot

Pickett plot has been used for computation of cementation factor and reservoir parameters of hydrocarbon-bearing formations penetrated through six wells; CBV, CPT, CMT, CNL, CPV and CKK in the Cauvery basin.

Water saturation computation for clean sand requires cementation factor (m), formation water resistivity (R_w), tortuosity (a) and saturation exponent (n). Therefore, the Pickett plot has been utilized obtaining aR_w and m from porosity, deep resistivity logs for all six wells. R_w values are

calculated from the spontaneous potential (SP) log for the selected intervals of six wells. This value is used for estimating ‘ a ’ in table 3. Water saturation is computed with the estimated aR_w and m from the Pickett plot for each well. For estimation of petrophysical constant like cementation factor (m) and reservoir parameters such as permeability is discussed through a well CKK below:

Pickett plot is generated using Archie’s formulae (Archie 1942). Rearranging the Archie equation we get

$$\text{Water saturation } (S_w) = I^{-1/n}, \quad (4)$$

where the resistivity index = I and saturation exponent = n .

$$I = R_t/R_0 \quad (R_0 = FR_w), \quad (5)$$

where

$$\text{Formation factor } (F) = a\Phi_t^{-m}, \quad (6)$$

and a is tortuosity and Φ_t = total porosity. $R_t = RD$, R_0 = resistivity of formation with 100% water saturation.

Equations (5 and 6) are combined to yield

$$\text{Resistivity } (R_t) = a\Phi_t^{-m} R_w I = a\Phi_t^{-m} R_w S_w, \quad (7)$$

where, R_w is the formation water resistivity.

Equation (7) (Pickett 1966) leads to

$$\text{Log } R_t = -m \text{log } \Phi_t + \text{log } (aR_w) + \text{log } I, \quad (8)$$

which is a straight line on log–log graph paper with slope ($-m$) and intercept (aR_w).

An example from a well CKK in Bhuvanagiri formation is shown in figure 8. The intercept is shown in this figure with total porosity (Φ_t) = 1. According to Pickett (1973), the saturation exponent ‘ n ’ which is a function of water saturation equals the value of porosity exponents ‘ m ’. Water

Table 2. *MLFN predicted results for five wells CKK, CPT, CPV, CKP and CBV.*

Well CKK/ depth (m)	Remarks	Well CPT/ depth (m)	Remarks	Well CPV/ depth (m)	Remarks
1075–1530	Shale	1750–2010	Shale	1575–1649.5	Shale
1530–1536	wbz	2010–2085	Shale and wbz	1649.5–1651.5	HC
1536–1642	Shale	2085–2150	Shale	1651.5–1652.5	wbz
1642–1650	wbz	2150–2240	Shale and wbz	1652.5–1685	Shale
1650–1740	Shale	2240–2310	Shale	1685–1703	Shale and wbz
1740–1744	wbz	2310–2345.5	wbz	1703–1759	Shale
1744–1784	Shale	2345.5–2347.5	HC	1759–1761	wbz
1784–1796	wbz	2347.5–2358	wbz	1761–1796	Shale
1796–1839	Shale	2358–2366.5	Shale	1796–1800	wbz
1839–1852	wbz	2366.5–2368.5	HC	1800–1811	Shale
1852–1870	Shale	2368.5–2370	wbz	1811–1813	wbz
1870–1879	wbz	2370–2392	Shale and wbz	1813–1903	Shale and wbz
1879–1957	Shale	2392–2420	Shale and wbz	1903–1912	Shale
1957–1965	HC	2420–2450	wbz	1912–1915	Shale and wbz
1965–1972	Shale	2450–2590	Shale and wbz	1915–1930	Shale
1972–1973	HC	2590–2650	wbz	1930–1937	wbz
1973–1974	Shale	2650–2680	Shale	1937–1945	Shale
1974–1987	HC	2680–2770	Shale and wbz	1945–2022	wbz
1987–1992	Shale	2770–2845	wbz	2022–2049	Shale
1992–2004	HC	2845–2863	Shale	2049–2058	wbz
2004–2015	Shale	2863–2940	Shale and wbz	2058–2082	Shale
2015–2034	HC	2940–2985	Shale and wbz	2082–2112	wbz
2034–2044	Shale	2985–3040	wbz	2112–2168	Shale
2044–2048	HC	3040–3089	Shale and wbz	2168–2190	Shale and wbz
2048–2051	Shale	3089–3090	HC	2190–2203	Shale
2051–2053	HC	3090–3325	wbz	2203–2210	wbz
2053–2065	Shale	3325–3326.5	HC	2210–2548	Shale
2065–2069	HC	3326.5–3330	wbz	2548–2550	HC
2069–2098	Shale	3330–3355	Shale and wbz	2550–2551	wbz
2098–2100	wbz	3355–3450	wbz	2551–2554	Shale
2100–2105	Shale	3450–3516	wbz	2554–2556	wbz
		3516–3518	HC	2556–2563	Shale
		3518–3520	Shale	2563–2569	wbz
		3520–3522	HC	2569–2578	Shale
		3522–3600	Shale and wbz	2578–2658.5	Shale and wbz
		3600–3601	HC	2858.5–2660	HC
		3601–3603	Shale	2660–2663	wbz
		3603–3604.5	HC	2663–2757	Shale and wbz
		3604.5–3665	Shale and wbz	2757–2759	HC

saturation lines varying from 25 to 100% are drawn in this plot. Table 3 lists the value of R_w , m for hydrocarbon bearing zones of six wells.

5.2 Permeability

The ability of rock to allow fluids to flow through interconnected pore space is termed as permeability (K). The irreducible water saturation (S_{wi}) is expressed as (Morries and Biggs 1967):

$$K^{1/2} = 250 \Phi_t^3 / S_{wi} \quad \text{for oil,} \quad (9a)$$

$$K^{1/2} = 79 \Phi_t^3 / S_{wi} \quad \text{for gas,} \quad (9b)$$

where S_{wi} is the irreducible water saturation.

The irreducible water saturation has been expressed in terms of total porosity and effective porosity (Aguilera 1990) as:

$$S_{wi} = \Phi_t * S_w / \Phi_{eff}. \quad (10)$$

Table 2. (Continued.)

Well CPV/ depth (m)	Remarks	Well CKP/ depth (m)	Remarks	Well CBV/ depth (m)	Remarks
2759–2774	wbz	1320–1756	Shale	3380–3402	wbz
2774–2775.5	HC	1756–1758	wbz	3402–3408	Shale
2775.5–2792	wbz	1758–1770	Shale	3408.3–3410	HC
2792–2803	Shale and wbz	1770–1771.5	wbz	3410–3413	Shale
2803–2817	Shale	1771.5–1784	Shale and wbz	3413–3416	wbz
2817–2835	Shale and wbz	1784–1859	Shale	3416–3421	Shale
2835–2885	wbz	1859–1863	wbz	3421–3425	wbz
2885–2901	Shale and wbz	1863–1867	Shale	3425–3427	Shale
2901–2906	wbz	1867–1885	Shale and wbz	3427–3433	wbz
2906–2935	Shale	1885–1922	Shale	3433–3435	HC
2935–2960	Shale and wbz	1922–1924	wbz	3435–3458	wbz
2960–2972	wbz	1924–1988	Shale	3458–3459	HC
2972–2992	Shale and wbz	1988–1989	wbz	3459–3462	wbz
2992–3007	Shale and wbz	1989–2028	Shale and wbz	3462–3464	HC
3007–3025	Shale	2028–2073	wbz	3464–3514	wbz
3025–3030	wbz	2073–2108	Shale	3514–3524	Shale
3030–3072	Shale	2108–2111	wbz	3524–3570	wbz
3072–3073	HC	2111–2118	Shale	3570–3572	Shale
3073–3075	wbz	2118–2148	wbz		
3075–3090	Shale and wbz	2148–2151	Shale		
3090–3091.5	HC	2115–2170	wbz		
3091.5–3106	Shale	2170–2215	Shale and wbz		
3106–3112	wbz	2115–2228	Shale		
3112–3135.5	Shale	2228–2236	wbz		
3135.5–3137	HC	2236–2247	Shale		
3137–3139	wbz	2247–2252	wbz		
3139–3279	Shale	2252–2258	Shale and wbz		
3273–3281	HC	2258–2269	Shale		
3281–3333	Shale	2269–2281	wbz		
3333–3336.5	wbz	2281–2297	wbz		
3336.5–3340	HC	2297–2350	Shale		
3340–3341	wbz	2350–2377	Shale and wbz		
3341–3372	Shale	2377–2398	Shale		
		2398–2999	wbz		
		2399–2404	Shale		
		2404–2406	wbz		
		2406–2415	Shale		
		2415–2417	wbz		
		2417–2437	Shale		
		2437–2480	wbz		

Wbz: Water bearing zone and HC: hydrocarbon bearing zone.

After incorporating into equation (7) the true resistivity in terms of permeability is written as (Aguilera 1990):

$$R_t = a\Phi_t^{-3n-m}R_w\left(250/K^{1/2}\right)^{-n} \quad \text{for oil,} \quad (11a)$$

$$R_t = a\Phi_t^{-3n-m}R_w\left(79/K^{1/2}\right)^{-n} \quad \text{for gas.} \quad (11b)$$

By taking logarithm on both sides for gas bearing zones in well CKK, equation (11b) is written as:

$$\begin{aligned} \text{Log } R_t &= (-3n-m) \log \Phi_t \\ &+ \log \left[aR_w \left(79/K^{1/2} \right)^{-n} \right]. \end{aligned} \quad (12)$$

From equation (12), by plotting R_t vs. Φ_t on log-log graph paper, the relation results a straight line with a slope equal to $(-3n - m)$ with a constant aR_w and permeability. Since $m = n$, the slope equals $(-4m)$. The intercept of a straight line with 100% porosity indicates $aR_w (79/K^{1/2})^{-n}$. The line of

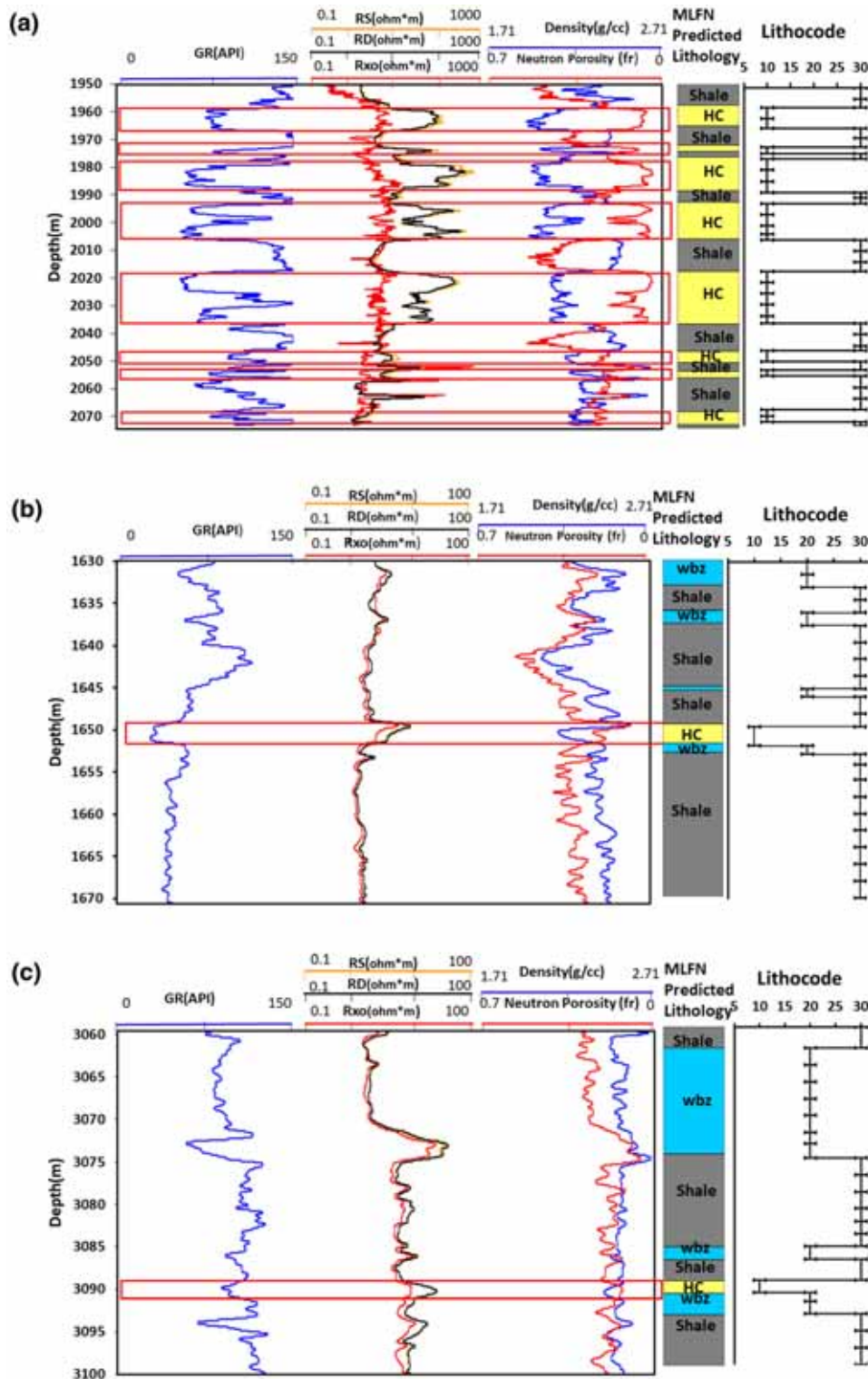


Figure 7. MLFN predicted results and their standard error bar with MLFN predicted lithology. (a) For depth interval 1950–2070 m in well CKK (standard error is 1.36), (b) for depth interval 1630–1670 m for well CPV (standard error is 1.06), (c) for depth interval 3060–3100 m for well CPV (standard error is 1.12), (d) for depth interval 3250–3350 m for well CPV (standard error is 0.99), and (e) for depth interval 3400–3440 m for well CBV (standard error is 1.13). HC: Hydrocarbon bearing zone, wbz: water bearing zone.

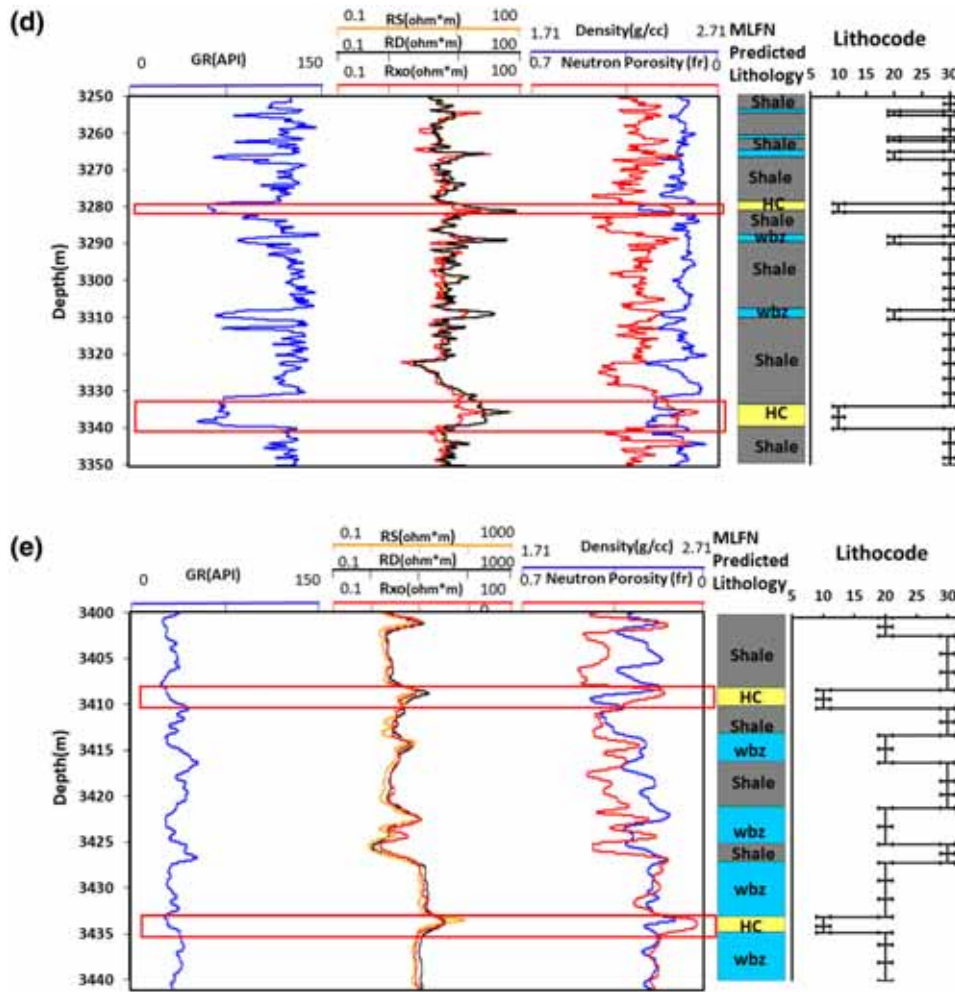


Figure 7. (Continued.)

constant permeability equals to 0.01 to 500 md is drawn by computing R_t from equation (11).

The parallel lines of permeability ranging from 0.01 to 500 md are shown in figure 9.

5.3 Estimation of volume of shale, porosity and water saturation

Hydrocarbon bearing zones are available in six wells under the study are of the Cauvery basin. Petrophysical parameters are estimated from six wells holding hydrocarbon bearing sediments, namely, CBV, CMT, CNL, CPV, CPT and CKK (figure 1). Table 4 shows the depth intervals of hydrocarbon bearing sediments from Niravai Sandstone aging Upper Oligocene to Andimadam formation of Lower Cretaceous from six wells. The thickness of hydrocarbon bearing zones ranges from 1 to 19 m. Table 4 lists the values of

petrophysical parameters of oil and gas bearing zones like effective porosity Φ_{eff} , the volume of shale (V_{sh}) and water saturation (S_w) of six wells in the Cauvery basin. The volume of shale and effective porosity (Φ_{eff}) are estimated from the following equations (Fertl and Frost 1980):

$$V_{\text{sh}} = \frac{(\text{GR} - \text{GR}_{\text{min}})}{(\text{GR}_{\text{max}} - \text{GR}_{\text{min}})}, \quad (13)$$

where GR = gamma ray log reading at any depth, GR_{min} = minimum gamma ray reading, and GR_{max} = maximum gamma ray reading. GR_{min} varies from 17 to 26 API and GR_{max} from 142 to 182 API in six wells.

$$\Phi_{\text{eff}} = \Phi_t * (1 - V_{\text{sh}}). \quad (14)$$

We have assumed clean sand when $V_{\text{sh}} \leq 6\%$ for computation of water saturation using Archie's law (Archie 1942).

Table 3. *Petrophysical constants and permeability estimated from Pickett plot for selected depth intervals of six wells in Cauvery basin.*

No.	Well name	Depth interval (m)	aRw	a	m	Permeability (md)	Lithology
1	CBV	3400–3464	0.19	1.45	1.5	1–300	Mainly argillaceous sandstone with minor shale, calcareous sandstone
2	CPT	2345–2369	0.037	1.45	1.66	10–100	Dominantly silty claystone and sand
		3080–3099	0.016	1.45	1.69	0.1–200	Mainly sandstone with minor shale alteration
		3320–3329	0.022	1	1.86	0.1–300	
		3516–3529	0.03	1.45	1.56	0.01–400	
		3600–3605	0.024	1.45	1.73	0.1–300	
3	CMT	418–570	0.14	1.45	1.8	10–100	Sandstone/claystone alternations with minor limestone
4	CNL	2083–2112	0.05	1.45	1.55	0.1–300	Sandstone and calcareous sandstone
5	CPV	1645–1655	0.14	1.65	1.31	10–90	Mainly sandstone with minor shale
		3090–3281	0.28	1.65	1.31	10–100	Mainly sandstone with minor shale
		3330–3340	0.16	1.45	1.55	10–200	Calcareous sandstone
6	CKK	1957–2069	0.016	1.45	1.75	0.1–400	Sandstone with shale

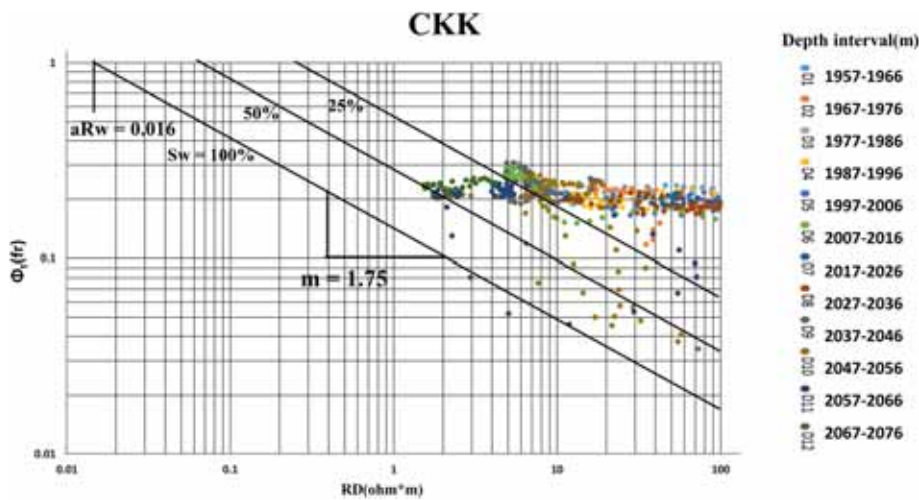


Figure 8. Pickett plot for the well CKK showing the water saturation lines and cementation factor.

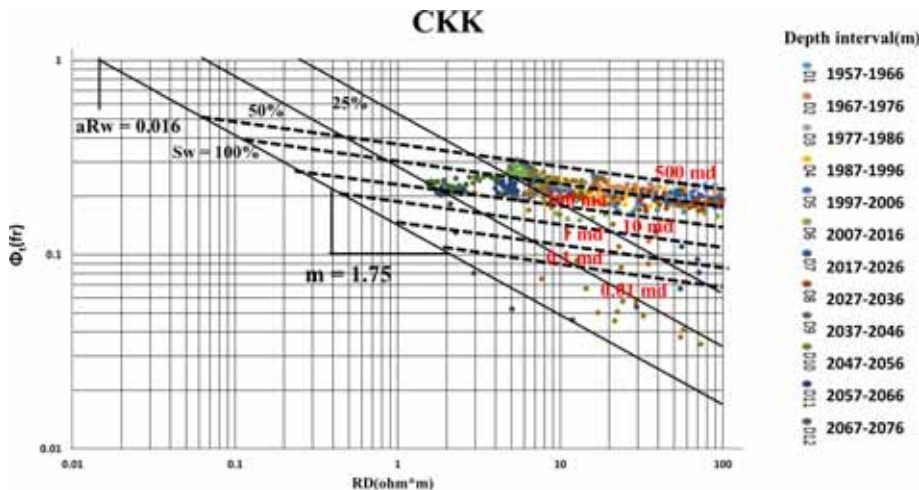


Figure 9. Pickett plot incorporating formation permeability for the well CKK.

Table 4. Petrophysical parameters for hydrocarbon bearing zones for six wells in Cauvery basin.

Wells	Hydrocarbon bearing zone				Petrophysical parameters							Field name	Formation	Geological age
	Depth interval (m)	Thickness (m)	Resistivity (Ωm) $\frac{R_{xo}}{RD}$	V_{sh} (%)	Effective porosity (%)	Water saturation (%)	Fluid type							
CBV	3408.3-3410	1.7	6	11	5	21	42	Oil	Bhuvanagiri	Bhuvanagiri Formation	Upper Cretaceous			
	3433-3434.7	1.7	20	30	0	10	45							
	3458-3459	1	9	12	6	15	50							
	3462-3464	2	12	20	6	13	55							
	2345.5-2347.5	2	1	5	0	26	45	Oil	Panampatti	Nannilam Formation and Bhuvanagiri Formation	Upper Cretaceous			
CPT	2366.5-2368.5	2	2	6	0	20	60							
	3089-3090	1	-	6	0	24	55							
	3325-3326.5	1.5	-	11	0	30	30							
	3516-3518	2	-	15	2	25	31							
	3520-3522	2	-	17	0	22	35							
	3600-3601	1	-	10	0	22	40							
	3603-3604.5	1.5	-	20	0	18	38							
	418.5-420	1.5	8	18	5	33	35	Oil	Mattur	Niravi Sandstone and Nannilam Formation	Upper Oligocene and Upper Cretaceous			
	567-570	3	5	7	0	30	60							
	1076.6-1079.6	3	10	16	5	18	55							
CNL	2083.5-2087.5	4	3	16	0	25	25	Gas	Nannilam	Nannilam Formation	Upper Cretaceous			
	2095-2112	17	5	25	0	25	30							
CPV	1649.5-1651.5	2	2	5	0.0	23	44	Oil & gas	Peruvalandan	Nannilam Formation, Bhuvanagiri and Andimadam Formation	Upper and Lower Cretaceous			
	3090.2-3091.5	1.3	6	21	5	11	50							
	3279.5-3281	1.5	13	50	2	19	25							
	3336.6-3340.8	4.2	12	30	6	15	30							
CKK	1957-1965	8	7	113	0.0	22	18	Gas	Kavilkalappal	Bhuvanagiri Formation	Lower Cretaceous			
	1972-1973	1	5	64	0.0	22	25							
	1974-1985	11	6	282	0.0	22	12							
	1985-1987	2	8	25	0.0	21	35							
	1992-2004	12	9	140	0.0	21	18							
	2015-2034	19	7	129	0.0	20	19							
	2044-2048	4	3	14	0.0	24	30							
2051-2053	2	3	11	0.0	22	35								
2065-2069	4	2	4	6	20	59								

6. Results and discussion

Hydrocarbon (HC) bearing zones are represented by the crossover between density and neutron porosity logs characterising high resistivity with low gamma ray value. Water saturation zones are represented as coinciding density and neutron porosity logs with low gamma ray and R_t value. Shale zones are represented by high neutron porosity (approx. 40%), low resistivity value with high gamma ray value. In general, the MLFN predicted model detects the water bearing, HC bearing zones and shale. The model is not able to detect other lithologies such as limestone or dolomites in these wells. There is a very good match between MLFN predicted HC bearing zones and quick look log interpretation at depths: 1950–2070 m in well CKK. Well CPV has shown very good match with the log data and MLFN predicted HC bearing zones namely; 1649.5–1651.5, 3090–3091.5, 3279.5–3281 and 3336.6–3380.8 m. Well CBV has shown good match with the log data and MLFN predicted HC bearing zones namely, 3408.3–3410, 3433–3434.7 m. MLFN predicted hydrocarbon bearing zones are listed for well CPT in table 2.

The cementation factor used in Archie's relation is an important parameter for the computation of water saturation. Its value generally varies from 1.3 to 3.1 depending on both reservoir and geological parameters (Salem and Chilingarian 1999; Tabibi and Emadi 2003). The lithologies of the selected hydrocarbon bearing zones of six wells are listed in table 3. The HC bearing zones are occurring in geological formations such as: Andimadam to Niravi Sandstone aging Lower Cretaceous to Upper Oligocene (table 4). The volume of shale in these zones is varying between 0 and 6%. Clean sands are assumed with V_{sh} less than 5–6%. Effective porosity and water saturation ranges from 10–33% and 12–60%, respectively. Cementation factor (m) in three wells, namely; CKK, CBV and CPV in Bhuvanagiri formation aging Lower Cretaceous to Upper Cretaceous ranges from 1.31 to 1.75 with porosity 10–24%. Oil bearing zones identified in wells CMT and CNL penetrated through Niravi Sandstone followed by Nannilam formation of Upper Oligocene to Upper Cretaceous characterize m varying from 1.55 to 1.80 with porosity 18–33%, respectively. Oil bearing sand layer in well CPT belonging to Nannilam and Bhuvanagiri formations of Upper Cretaceous indicates varying m of 1.56 to 1.86 with 18–30% porosity. Andimadam formation of Lower

Cretaceous penetrated by a well CPV indicates m of 1.55 with the porosity of 11–19% whereas other penetrated gas and oil bearing zones in Bhuvanagiri and Nannilam formations are characterized by low m of 1.31. The value of m is found to be 1.8–1.86 in high porous sands and 1.31 in low porous sands. Permeability ranges from 0.01 to 400 md of these wells. Low permeability is observed in oil well CPV and the highest permeability is observed in gas well CKK, respectively.

Several publications are available to predict the petrophysical parameters: porosity, permeability, water saturation, the volume of shale, lithofacies using neural network modelling (Anifowose *et al.* 2016; Gogoi and Chatterjee 2019). The key findings of this paper are to detect HC zones from well log data and to estimate shale volume, porosity, water saturation and permeability for these HC zones. The porosity, permeability and volume shale values of sandstone reservoirs in Andimadam, Bhuvanagiri, Nannilam and Niravi formations are adequate to hold sufficient hydrocarbon. These reservoir characteristics tend to improve significantly as sedimentation proceeds basinwards. Very good quality reservoir characterizing with porosity 20–22% and permeability of 300–400 md exists in well CKK of Bhuvanagiri formation.

Petrophysical analyses are crucial to reservoir modelling because the physical parameters of rocks provide a reference for delineating reservoir and non-reservoir distributions (El sayed *et al.* 1993; Bornard *et al.* 2005). Reservoir characterization has been carried out using conventional well log data of Abu Madi Formation in Abu Madi and El Qar'a fields, Nile delta Egypt to predict information about porosity, the volume of shale and hydrocarbon saturation (Mahmoud *et al.* 2017). Petrophysical parameters had been calculated using well log data in Krishna–Godavari and Upper Assam basin (Das and Chatterjee 2018; Gogoi and Chatterjee 2019). Reservoir discrimination and characterization of its lithology along with its fluid-content in reservoirs of Cauvery basins uses quantitative techniques of log studies. These factors along with seismic data will discriminate the reservoirs and non-reservoirs under the study area. However, the identification of HC zones from well log data using MLFN modelling in the Cauvery basin would be useful as a tool for the classification of lithology and HC zones for other sedimentary basins of India. These studies would further be implemented for reservoir modelling in

addition with seismic data (Datta Gupta *et al.* 2012).

7. Conclusions

This paper reveals the ability of MLFN modelling in the classification of lithology from well log data. Complex lithologies consisting of sandstone, limestone, dolomite and shale exist in these sediments penetrated through the wells. The methodology discussed demonstrates the classification of sands in terms of hydrocarbon and water bearing zones along with shale using MLFN model from two training wells. The MLFN model is tested for identification of HC zones for the other four wells, CKK, CPV, CBV and CPT. MLFN model is not used for well CKL as it lacks neutron porosity data. Out of the seven wells, HC zones are identified from six wells using the MLFN model. Petrophysical parameters are obtained from these zones. Pickett plot technique is found to be useful for the computation of cementation factor, formation water resistivity, tortuosity, saturation exponent and permeability from well log data. The thickness of 30 HC zones in six wells varies from 1 to 19 m. Clean sands are interpreted in terms of effective porosity and water saturation estimation. Sand with high porosity (30–33%) present in wells CMT and CPT shows a higher m (1.8–1.86) whereas sand with low porosity (~11%) in well CPV indicates a low m of 1.31. The petrophysical analysis shows that the reservoir in Bhuvanagiri formation is of very good quality with hydrocarbon saturation ranging from 40 to 88%, the volume of shale between 0 and 6% followed by a good quality reservoir in Niravi, Nannillam and Andimadam formations with hydrocarbon saturation 60–70%. In the Petroleum industry, this method is suitable and plays a substantial role in lithology classification in the exploration stage.

Acknowledgement

We are sincerely thankful to ONGC for providing the well log data for academic and research work.

References

- Aguilera R 1990 Extension of Pickett plots for the analysis of shaly formation by well logs; *Log Analyst* **31**(6) 304–313.
- Aguilera R 2001 Incorporating capillary pressure, pore throat aperture radii, height above free-water table and Winland r_{35} values on Pickett plots; *AAPG Bull.* **86**(4) 605–620.
- Aguilera R and Aguilera M S 2002 The integration of capillary pressures and Pickett plots for determination of flow units and reservoir containers; *SPE Reserv. Eval. Eng.* **5**(6) 465–471.
- Anifowose F, Adeniyi S, Abdulraheem A and Al-Shuhail A 2016 Integrating seismic and log data for improved petroleum reservoir properties estimation using non-linear feature-selection based hybrid computational intelligence models; *J. Pet. Sci. Eng.* **145** 230–237.
- Archie G E 1942 The electrical resistivity logs as an aid in determining some reservoir characteristics; *Trans. AIME* **146**(01) 54–67.
- Baldwin J L, Bateman R M and Wheatley C L 1990 Application of a neural network to the problem of mineral identification from well log; *Log Analyst* **3** 279–293.
- Bateman R M 1985 Openhole log analysis and formation evaluation, Prentice Hall PTR, New Jersey, 647p.
- Bhatt A and Helle H B 2002 Determination of facies from well logs using modular neural networks; *Petrol. Sci.* **8** 217–228.
- Bornard R, Allo F, Coléou T, Freudenreich Y, Caldwell D H and Hamman J G 2005 Petrophysical seismic inversion to determine more accurate and precise reservoir properties; SPE Europec Madrid, June 13–16, SPE 94144, <https://doi.org/10.2118/94144-MS>.
- Choudhury B, Das M and Singha S 2015 Well log analysis and reservoir characterization using Pickett's Plot Modeling; Presented in 11th Biennial International Conference & Exposition, SEG, India, Jaipur, Rajasthan, Dec. 4–6.
- Chatterjee R, Singha D, Ojha M, Sen M and Sain K 2016 Porosity estimation from pre-stack seismic data in gas-hydrate bearing sediments, Krishna–Godavari basin, India; *J. Nat. Gas Sci. Eng.* **33** 562–572.
- Das B and Chatterjee R 2018 Well log data analysis for lithology and fluid identification in Krishna–Godavari Basin, India; *Arab. J. Geosci.* **11** 231–242.
- Datta Gupta S, Chatterjee R and Farooqui M Y 2012 Rock physics template (RPT) analysis of well logs and seismic data for lithology and fluid classification in Cambay basin; *Int. J. Earth Sci.* **101**(5) 1407–1426.
- Dayoff J E 1990 *Neural network architectures: An introduction*; New York City: Van Nostrand Reinhold.
- Eichkitz C G, Schreilechner M G, Amtmann J and Schmid C 2009 Shallow seismic reflection study of the Gschliefgraben landslide deposition area interpretation and three dimensional modeling; *Aust. J. Earth Sci.* **102** 52–60.
- El-Khadrag A A, Ghorab M A, Shazly T F, Ramadan M and El-Sawy M Z 2014 Using of Pickett's plot in determining the reservoir characteristics in Abu Roash Formation, El Razzak Oil Field, North Western Desert, Egypt; *Egypt. J. Petrol.* **23**(01) 45–51.
- El Sayed A M A, Mouse S A, Higazi A and Al-Kodsh A 1993 Reservoir characteristics of the Bahariya Formation in both Salaam and Khalda oil fields, Western Desert, Egypt; *E.G.S. Proc. 11th Ann. Mtg.* **11** 115–132.
- Fertl W and Frost E 1980 Evaluation of shaly classic reservoir rocks; *J. Petrol. Technol.* **32**(09) 1641–1645.
- Ghosh S, Chatterjee R and Shanker P 2016 Estimation of ash, moisture content and detection of coal lithofacies from well

- logs using regression and artificial neural network modelling; *Fuel* **177** 279–287.
- Gogoi T and Chatterjee R 2019 Estimation of petrophysical parameters using seismic inversion and neural network modeling in upper Assam Basin, India; *Geosci. Frontiers* **10(03)** 1113–1124.
- Greengold G E 1986 The graphical representation of bulk volume of water on the Pickett crossplot; *Log Analyst* **27(3)** 1–25.
- Hampson D, Schuelke J and Quirein J 2001 Use of multi-attribute transforms to predict log properties from seismic data; *Geophysics* **66** 220–236.
- Lim J 2005 Reservoir properties determination using fuzzy logic and neural networks from well data in offshore Korea; *J. Petrol. Sci. Eng.* **49** 182–192.
- Maiti S, Tiwari R K and Kumpel H J 2007 Neural network modelling and classification of lithofacies using well log data: A case study from KTB borehole site; *Geophys. J. Int.* **169** 733–746.
- Mahmoud M, Ghorab M, Shazly T, Shibl A and Abuhagaza A A 2017 Reservoir characterization utilizing the well logging analysis of Abu Madi Formation, Nile Delta, Egypt; *Egypt. J. Petrol.* **26** 649–659.
- Martin A J, Solomon S T and Hartmann D J 1997 Characterization of petrophysical flow units in carbonate reservoirs; *AAPG Bull.* **81(5)** 734–759.
- Masoudi P, Tokhmechi B, Zahedi A and Jafari M A 2011 Developing a method for identification of net zones using log data and diffusivity equation; *J. Mining Environ.* **2(1)** 53–60.
- Masters T 1994 *Signal and Image Processing with Neural Networks*; Wiley & Sons, New York.
- Morries R L and Biggs W P 1967 Using log-derived values of water saturation and porosity; Presented in SPWLA 8th Annual Logging Symposium, Denver, Colorado, 12–14 June.
- Paul S, Ali M and Chatterjee R 2018 Prediction of compressional wave velocity using regression and neural network modeling and estimation of stress orientation in Bokaro Coalfield, India; *Pure Appl. Geophys.* **175(1)** 375–388.
- Phaye D K, Nambian M V and Srivastava D K 2011 Evaluation of petroleum system of Ariyalur–Pondicherry sub-basin (Bhuvavgiri area) of Cauvery Basin, India: A two dimensional (2-D) basin modelling study; Presented in 2nd South Asian Geoscience Conference and Exhibition GeoIndia, Greater Noida, New Delhi, India, 12–14 January.
- Pickett G R 1966 A review of current techniques for determination of water saturation from log; *J. Petrol Technol.* **18(11)** 1425–1433.
- Pickett G R 1973 Pattern recognition as a means of formation evaluation; Presented in SPWLA 14th Annual Logging Symposium Transactions, Lafayette, Louisiana, 6–9 May, Paper A, A1–A21.
- Prabhakar K N and Zutshi P L 1993 Evaluation of southern part of Indian east coast basins; *J. Geol. Soc. India* **41** 215–230.
- Rider M H 2002 *The Geological Interpretation of Well Logs* (2nd edn); Rider and French Consulting Limited, Scotland Interprint Ltd., Malta.
- Saha G C, Borhtakur A and Chaudhuri A 2008 A case study on log property mapping in Ramnad Sub-basin for better understanding the Nannilam Reservoir distribution and risk reduction in exploration; Presented in SPG 7th Biennial Conference and Exposition on Petroleum Geophysics, Hyderabad, India, 14–16 January, SPG-173-MS.
- Salem H S and Chilingarian G V 1999 The cementation factor of Archie's equation for shaly sandstone reservoirs; *J. Petrol. Sci. Eng.* **23(02)** 83–93.
- Sanyal S K and Ellithorpe J E 1978 A generalized resistivity–porosity cross plot concept; Presented in SPE Regional Meeting, San Francisco, California, 12–14 April, SPE-7145-MS.
- Schlumberger 1972 The essentials of log interpretation practice; Services Techniques Schlumberger, 58p.
- Schmitt P, Veronez M R, Tognoli F M W, Todt V, Lopes R C and Silva C A U 2013 Electrofacies modelling and lithological classification of coals and mud bearing ingrained siliciclastic rocks based on neural networks; *Earth Sci. Res. J.* **2** 193–208.
- Singha D and Chatterjee R 2017 Rock physics modeling in sand reservoir through well log analysis, Krishna–Godavari basin, India; *Geomech. Eng.* **13(1)** 99–117.
- Singha D K, Chatterjee R, Sen M K and Sain K 2014 Pore pressure prediction in gas-hydrate bearing sediments of Krishna–Godavari Basin in India; *Marine Geol.* **357** 1–11.
- Tabibi M and Emadi M A 2003 Variable cementation factor determination (empirical methods); Presented in 13th Middle East Oil Show and Conference, Bahrain, 5–8 April, SPE-81459-MS.
- Venkatarengan R, Prabhakar K N, Singh D N, Awasthi A K, Reddy P K, Mishra P K and Roy P K 1993 Lithostratigraphy of Indian petroliferous basin, Documente VII, Cauvery basin, KDM Institute petroleum exploration ONGC Dehradun, India, 31p (unpublished report).